Katabatic Winds on Ice Sheets: A Refinement of the Prandtl Model

R. J. ZAMMETT AND A. C. FOWLER

Mathematical Institute, Oxford University, Oxford, United Kingdom

(Manuscript received 29 August 2005, in final form 4 October 2006)

ABSTRACT

Katabatic winds on ice sheets and glaciers are buoyancy-driven flows, much like turbidity currents in the ocean. These winds are driven by radiative cooling of the ice surface and are not resolved by the typical horizontal and vertical discretization of general circulation models; therefore, a parameterization of their magnitude is desirable. In this paper, it is shown that the simplest such parameterization, based on the classical Prandtl model of slope winds, is physically inadmissible, and an improved model, which removes this irregularity, is presented. It is also shown that the improved model allows favorable comparison with both observations and regional numerical models.

1. Introduction

Katabatic winds are slope winds that occur over ice sheets and glaciers, and which arise due to the radiative cooling of the surface, which forms a layer of dense, cold air that flows down the ice slope under its own weight (Davolio and Buzzi 2002). These winds are remarkably unidirectional, and can be very persistent and strong (Parish and Waight 1987; King and Turner 1997). Typical depths of the katabatic wind layer are of the order of tens to hundreds of meters and, because of this, such winds are not well represented in atmospheric weather prediction models. It is thus of interest to derive approximate parameterizations of katabatic winds, both as inputs to GCMs, and also to serve as inputs to models of other processes which involve surface winds, such as the wind-blown erosion and transport of snow, and the formation of mega-dunes and sastrugi.

The simplest model of a katabatic wind is perhaps that of Prandtl (1952), who considered the advection and turbulent diffusion of momentum and sensible heat in a gravity current. Slightly more detailed is the model of Ball (1956, 1960), which allows for along-slope variations of temperature and wind speed. While there is little doubt that momentum and sensible heat transport are the dominant factors in the formation and maintenance of katabatic winds, other factors may also be important. Of these, moisture transport and the effects of rotation will have a quantitative effect. In Antarctica, and perhaps other continental ice sheets such as the former Laurentide ice sheet, the atmosphere is dry, and moisture advection is unimportant. The Coriolis force is significant when the Rossby number $U/\Omega L$ is less than 1. If we take $U = 20\ \mathrm{m\ s^{-1}}$ and $\Omega = 0.7 \times 10^{-4}\ \mathrm{s^{-1}}$, this gives a length scale of some 280 km when the Rossby number is equal to 1. At the scale of an ice sheet, Coriolis forces become dominant.

The importance of rotation at large scales raises the question as to whether slope winds may be forced by the overlying geostrophic flow. A significant literature has developed over the last 20 years, which is concerned with the question of how slope winds over ice sheets are driven at these larger scales, since the features of unidirectionality and strength appear to penetrate far into the interior of the Antarctic ice sheet (e.g., Van Lipzig et al. 2004; Bromwich et al. 2001; Renfrew and Anderson 2002; Parish and Waight 1987). Mostly, high-resolution numerical models have been used to study this question, and these models are able to resolve the katabatic wind layer; they also agree favorably with observations (Parish and Cassano 2003; Lefebre et al. 2005; Heinemann and Klein 2002). In some cases, it appears that these external climatological factors have only a moderate influence on the surface winds (Bromwich et al. 1996), and the dominant balance in numerical models is also that of the Prandtl model between thermal buoyancy and surface drag

Corresponding author address: R. J. Zammett, Mathematical Institute, Oxford University, 24-29 St. Giles', Oxford OX1 3LB, United Kingdom.
E-mail: zammettr@maths.ox.ac.uk

DOI: 10.1175/JAS3960.1

(Nappo and Rao 1987; Skyllingstad 2003; Renfrew 2004).

A different approach to the study of katabatic winds arises when we seek to parameterize the flows (Oerlemans and Grisogono 2002), and this is the approach we take in this paper. We seek the simplest model that can credibly represent observations, since the aim is to provide an analytic solution that can provide an explicit representation of the momentum and heat fluxes. Our strategy in doing this is orthogonal to those of high-resolution regional models, insofar as we aim to build in complexity gradually rather than all at once. In this paper, we focus on the Prandtl model, which describes steady, pure katabatic flow. This model is of interest because it provides a simple analytic solution of the governing equations. The physical assumptions made are that the largest contributions to the momentum equation are frictional and buoyancy forces, while the largest contribution to the energy equation is sensible heat flux, assuming a stably stratified boundary layer. The classical Prandtl model assumes constant slope, eddy diffusivity, and thermal conductivity. As discussed above, these assumptions are qualitatively reasonable at least. Inclusion of the Coriolis force in the Prandtl model has been studied by Stiperski et al. (2007).

The Prandtl model also gives a reasonable fit to observed wind speed and potential temperature profiles (as we will also show below). The main problem with its solution is its inability to describe the sharp near-surface gradients of wind speed and potential temperature that are observed. This is attributed to its assumption of a constant mixing length, which is too large near the surface. This problem has been addressed both numerically, as in the model of Rao and Snodgrass (1981) for example, and analytically, using the WKB approximation,[1] by Grisogono and Oerlemans (2001), who found that there was a good agreement between their model results and those collected over Breidamerkurjökull (Parmhed et al. 2004). Hootman and Blumen (1983) compared the Prandtl model with that of Rao and Snodgrass as a fit for data collected in Colorado. They found that both models agreed well with data, but near surface temperatures were better simulated by the Rao and Snodgrass model. The fair agreement of the classical Prandtl solution with observations provides support for the underlying physics of the model.

The purpose of this paper is to point out and correct an anomaly in the parameterizations based on the classical Prandtl model. We illustrate our argument by analyzing the simplest model, but our argument will apply equally well to modified versions such as that studied by Grisogono and Oerlemans (2001, 2002; see also Grisogono 2003). The anomaly arises because the katabatic mass flux depends on the local slope in such a way that it becomes unbounded as the slope tends to zero. This error arises because the classical model ignores horizontal divergence, and its correction makes a significant change to the solution.

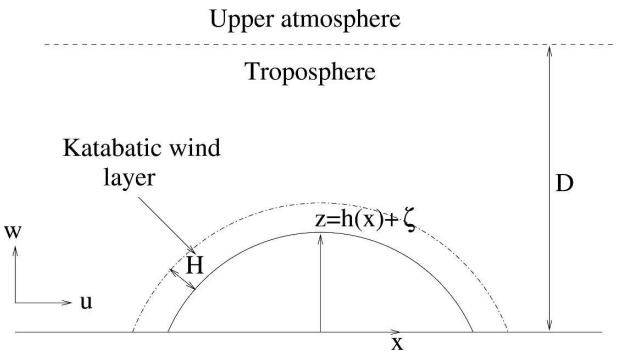

FIG. 1. Coordinate system in two dimensions.

In this paper, we modify the classical Prandtl model to allow for varying slope. For simplicity, we retain the assumptions of constant eddy diffusivity and thermal conductivity. To show that the corrected model is reasonable, we then compare both the classical and modified Prandtl solutions with data collected during the Katabatic Wind and Boundary Layer Front Experiment around Greenland during 1997 (KABEG'97) (Heinemann 1999), and numerical results obtained using the fifth-generation Pennsylvania State University–National Center for Atmospheric Research (PSU–NCAR) Mesoscale Model (MM5), adapted for use in a polar environment (Bromwich et al. 2001), and hereafter referred to as Polar MM5. Although we make this comparison to show that the parameterized model can fit observations, we do not seek to establish that in all circumstances, the neglect of moisture, Coriolis force, and external pressure gradient is quantitatively accurate.

2. The Prandtl model

We consider two-dimensional steady, irrotational, hydrostatic flow over an ice sheet of nonconstant slope using the (x, ζ) coordinate system shown in Fig. 1; thus u is the downslope component of the katabatic wind.

Conservation of mass, energy, and downslope momentum, together with the hydrostatic approximation

[1] The WKB approximation is an asymptotic method, which is used to solve linear differential equations with slowly varying coefficients; see Bender and Orszag (1978).

for the pressure, and neglecting Coriolis terms for simplicity, yields the system

$$\frac{d\rho}{dt} + \rho\nabla\cdot\mathbf{u} = 0, \tag{2.1}$$

$$\rho c_p \frac{dT}{dt} - \frac{dp}{dt} = \frac{\partial}{\partial\zeta}\left(k_V \frac{\partial T}{\partial\zeta}\right) + Q, \tag{2.2}$$

$$\rho \frac{du}{dt} = -\left(\frac{\partial p}{\partial x} - h_x \frac{\partial p}{\partial\zeta}\right) + \frac{\partial}{\partial\zeta}\left(\mu_V \frac{\partial u}{\partial\zeta}\right), \tag{2.3}$$

$$\frac{\partial p}{\partial\zeta} = -\rho g, \tag{2.4}$$

where $\mathbf{u} = (u, W)$, $W = w - uh_x$, $(d/dt) = (\partial/\partial t) + \mathbf{u}\cdot\nabla$ and $\nabla = [(\partial/\partial x), (\partial/\partial\zeta)]$; $k_V(z)$ is an effective thermal conductivity, $\mu_V(z)$ a dynamic eddy viscosity and Q represents radiative and latent heat transfer. Other symbols have their usual meaning. As the katabatic wind layer has a depth of $O(100\text{ m})$, we assume that the main mechanism of vertical heat transfer will be turbulent heat conduction. We also assume that the air in the katabatic wind layer is dry (reasonable away from the margins of an ice sheet), and thus advective latent heat transfer will be negligible.

Equations (2.1)–(2.3) coupled with the hydrostatic approximation and the perfect gas law are five equations for the five variables ρ, u, W, p, and T. To obtain suitable boundary conditions for T, we briefly consider the adiabatic temperature, $T_A(z)$, and density, $\rho_A(z)$: assuming a dry adiabat, we follow Fowler (2005) and use the following expressions

$$T_A(z) = T_0 - \frac{gz}{c_p}, \tag{2.5}$$

$$\rho_A(z) = \rho_0\left(1 - \frac{gz}{c_p T_0}\right)^{\frac{M_a c_p}{R} - 1}. \tag{2.6}$$

We note that on Earth, $(c_p T_0/g) \approx 29$ km and $(M_a c_p/R) \approx 3.4$; thus we approximate

$$\rho_A(z) \approx \rho_0 \exp\left(-z\frac{M_a g}{RT_0}\right), \tag{2.7}$$

where $(RT_0/M_a g) \approx 8.6$ km, the scale height of the atmosphere. Thus

$$\frac{\rho_A(z)}{T_A(z)} = \frac{\rho_0 \exp\left(-z\dfrac{M_a g}{RT_0}\right)}{T_0 - \dfrac{gz}{c_P}} \approx \frac{\rho_0}{T_0\left(1 - \dfrac{gz}{c_P T_0}\right)} \approx \frac{\rho_0}{T_0}. \tag{2.8}$$

In the midlatitudes, the size of Q relative to the advective terms is $O(\text{Ro}^2)$, where Ro is the Rossby number. The Rossby number is $O(10^{-1})$ for synoptic scales (see Pedlosky 1979), and thus Q is small (but nonzero). Ignoring the conductive term in Eq. (2.2), the near adiabatic tropospheric temperature satisfies

$$w_A(\rho_A c_p T'_A - p'_A) \approx Q, \tag{2.9}$$

where w_A is the vertical velocity in the troposphere, and a prime denotes differentiation with respect to z. We can write Q in terms of the Brunt–Väisälä frequency N, a measured quantity defined by

$$N^2 = \frac{g}{\theta}\frac{\partial\theta}{\partial z}, \tag{2.10}$$

where θ is the potential temperature. Using the definition $\theta = T(p_0/p)^{(R/M_a c_p)}$ (Pedlosky 1979) together with the perfect gas law $p = \rho RT/M_a$, some algebraic manipulation shows that

$$Q = w_A \frac{M_a c_p}{R}\frac{p_A}{g} N^2. \tag{2.11}$$

It is estimated that $N^2 = O(10^{-4})\ \text{s}^{-2}$ (Pedlosky 1979).

We prescribe the standard boundary conditions: at the ice cap surface, we use those of no slip and a specified temperature deficit below the local adiabatic temperature,

$$u = 0, \quad T = T_A[h(x)] - \Delta T \quad \text{on} \quad \zeta = 0. \tag{2.12}$$

We wish to match the solution within the katabatic wind layer to the solution in the planetary boundary layer, and we therefore pose matching conditions in the form

$$u \to 0, \quad T \to T_A[h(x)] \quad \text{as} \quad \zeta \to \infty. \tag{2.13}$$

a. Nondimensionalization

Using the cross section of the Greenland ice sheet shown in Figs. 2 and 3, we set $h_D(x) = h_0 + h(x)$, where $h_0 = 600$ m, in order that the dimensionless ice cap margin lies at $z = 0$. We write $T = T_A[h(x)] + (\Delta T)\tilde{T}$, where ΔT is a typical surface temperature deficit, and use the scales

$$u \sim U, \quad W \sim \frac{HU}{l}, \quad x \sim l, \quad z, h \sim D, \quad \zeta = H\xi,$$

$$p \sim p_0, \quad \rho \sim \rho_0, \quad T \sim T_0, \quad T_A \sim T_0, \quad t \sim \frac{l}{U}. \tag{2.14}$$

We now have (dimensionlessly) that $T = T_A + \delta\tilde{T}$, where $\delta = (\Delta T/T_0)$. We choose D by requiring

$$p_0 = \rho_0 g D = \frac{\rho_0 RT_0}{M_a}. \tag{2.15}$$

The scales U and H will be chosen below.

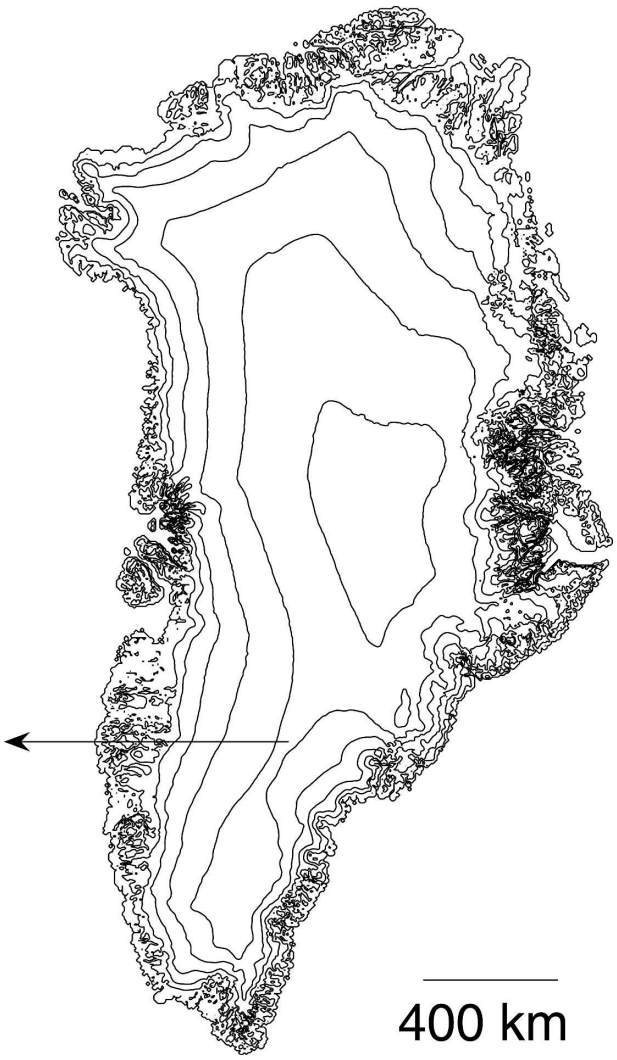

FIG. 2. Contour map of Greenland using data from the National Center for Snow and Ice Data (see Bamber et al. 2001; Layberry and Bamber 2001). Contours are plotted every 500 m; the highest contour corresponds to an elevation of 3000 m ASL. The horizontal line with the arrow indicates the cross section of the ice sheet passing through the location where the katabatic wind data was collected; the arrow denotes the direction of the cross section in Fig. 3.

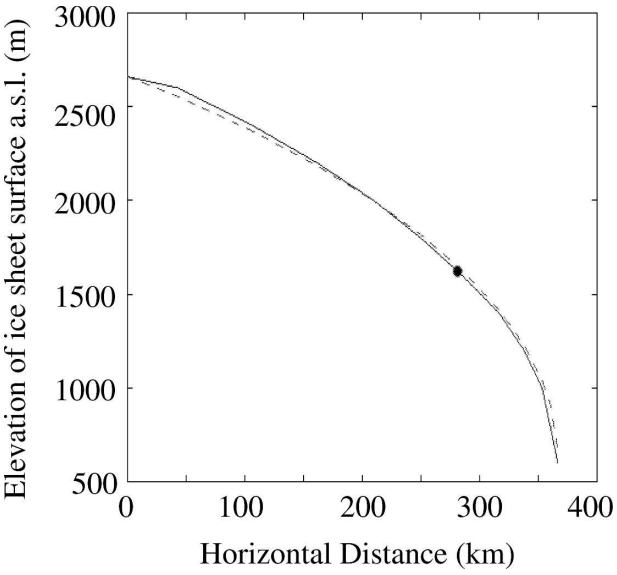

FIG. 3. Cross section through the west Greenland ice cap. The solid line indicates the cross section; the dashed line the approximation given by $h_D(x) = h_0 + a\{1 - b[(x/L)]^n\}^{1/m}$. The values used were $h_0 = 600$ m, $a = 2060$ m, $n = 1.05$, $m = 2.1$, $L = 3.67 \times 10^5$ m, and $b = 1$. This corresponds to $n = 20$ for Glen's flow law, and thus implies that flow is almost plastic (see Paterson 1994). Note that this is drawn moving from west to east (the direction of the arrow in Fig. 2). The circle denotes the location at which the data were collected (Heinemann 1999).

Defining $\varepsilon = (H/D)$, Eqs. (2.2), (2.3), and (2.4) become

$$\rho \frac{dT}{dt} - \alpha \frac{dp}{dt} = \left(\frac{\kappa_V l}{H}\right) \frac{\partial^2 T}{\partial \xi^2} + \lambda, \tag{2.16}$$

$$F^2 \rho \frac{du}{dt} = -\left(\frac{\partial p}{\partial x} - \frac{1}{\varepsilon} h_x \frac{\partial p}{\partial \xi}\right) + \frac{F^2 l \varepsilon_V}{H} \frac{\partial^2 u}{\partial \xi^2}, \tag{2.17}$$

$$\frac{1}{\varepsilon} \frac{\partial p}{\partial \xi} = -\rho, \tag{2.18}$$

where we define

$$\kappa_V = \frac{k_V}{\rho_0 c_p U H}, \quad \varepsilon_V = \frac{\mu_V}{\rho_0 U H}, \quad F^2 = \frac{U^2}{gD},$$
$$\alpha = \frac{R}{M_a c_p}, \quad \lambda = \frac{lQ}{\rho_0 c_p T_0 U}. \tag{2.19}$$

This assumes that $k_V(z)$ and $\mu_V(z)$ are constant; κ_V and ε_V are dimensionless turbulence coefficients of similar size that are comparable to the drag coefficient, estimated as $O(10^{-3})$–$O(10^{-4})$ over ice (Paterson 1994). In addition, we have the dimensionless perfect gas law

$$p = \rho T. \tag{2.20}$$

In dimensionless terms, Eq. (2.9) becomes

$$\rho_A T'_A - \alpha p'_A = \frac{QD}{w_A \rho_0 c_p T_0}, \tag{2.21}$$

where the prime now represents differentiation with respect to dimensionless z.

To estimate the size of λ in (2.16), we use (2.11) to write

$$\lambda = \frac{w_A l}{UD} \frac{p_A}{p_0} \frac{N^2}{(g/D)}. \tag{2.22}$$

Following Pedlosky (1979), we have $(w_A l/UD) \sim \mathrm{Ro}$, $[N^2/(g/D)] \sim \mathrm{Ro}$, and since $p_A \lesssim p_0$, we have $\lambda \sim \mathrm{Ro}^2 \sim 10^{-2}$. Consequently, we neglect the term λ in (2.16).

To calculate the order of magnitude of δ, we note that $\Delta T \sim 10$–20 K, (e.g., Heinemann 1999); given a reference temperature $T_0 = 273$ K, this gives a range of values for $\delta = 3.6$–7.3×10^{-2}. Using (2.12) and (2.13), the boundary conditions for $\tilde{T}$ are

$$\tilde{T} = -1 \quad \text{on} \quad \xi = 0, \quad \tilde{T} \to 0 \quad \text{as} \quad \xi \to \infty. \tag{2.23}$$

The boundary conditions for u are unchanged.

The choice of parameters here and below is made in order to be as realistic as possible, but it must be emphasized that in the real physical situation, the surface temperature (and thus δ) is not prescribed, but is determined through a radiative energy balance. Our choice of ΔT aims to reflect this, and we do not pursue more realistic boundary conditions for purposes of simplicity.

b. Simplification of equations

Assuming $\varepsilon \ll \delta$, noting $z \approx h(x)$, and setting

$$f^2 = \frac{H}{\varepsilon_V l}, \quad \mathrm{Pr}_T = \frac{\varepsilon_V}{\kappa_V}, \tag{2.24}$$

Eqs. (2.16) and (2.17) become, to leading order,

$$\beta u h_x + \mathrm{Pr}_T f^2 \left(\rho_A \frac{d\tilde{T}}{dt} - \rho_A \frac{T_A'}{T_A} u h_x \tilde{T} \right) = \frac{\partial^2 \tilde{T}}{\partial \xi^2}, \tag{2.25}$$

$$f^2 \rho_A \frac{du}{dt} - \nu \frac{\rho_A \tilde{T} h_x}{T_A} = \frac{\partial^2 u}{\partial \xi^2}, \tag{2.26}$$

where

$$\beta = \frac{H}{\delta \kappa_V l} \frac{N^2}{(g/D)} \frac{p_A}{p_0}, \quad \nu = \frac{\delta f^2}{F^2}, \tag{2.27}$$

and Pr_T is the turbulent Prandtl number, the ratio of the turbulent diffusivities. Note that we have used Eq. (2.21) and the definition of λ in (2.19) to remove the adiabatic temperature from the energy equation (2.25). The derivation of (2.25) and (2.26) from (2.16) and (2.17) involves the use of the hydrostatic approximation (2.18), which implies that $p \approx p_A[h(x)] + O(\varepsilon)$, together with the perfect gas law (2.20), from which we derive the approximation (with $p \approx p_A$)

$$\rho - \rho_A \approx -\frac{\delta \rho_A}{T_A} \tilde{T}. \tag{2.28}$$

We assume the value $\delta = 4.4 \times 10^{-2}$ and take $U = 21.5$ m s^{-1}, $H = 120$ m (see Fig. 4) and $D = 8.6$ km. We take $l = 367$ km, the length from the ridge to the ice cap edge along the flow line passing through the location of data collection. The Brunt–Väisälä frequency is taken as $N = 1.5 \times 10^{-2}$ s^{-1} (King 1989), and we take $p_A = p_0$.

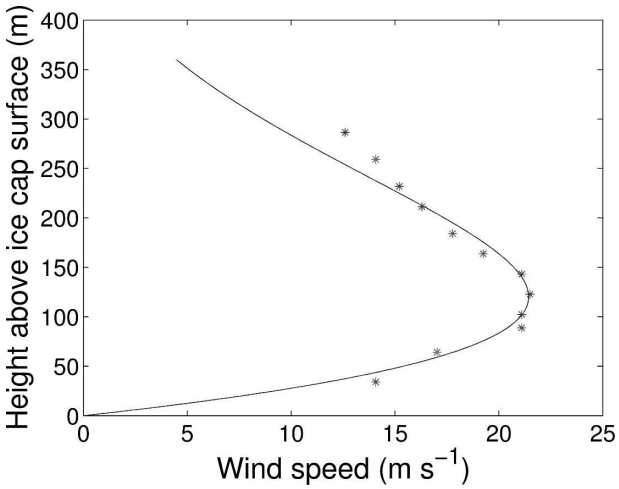

FIG. 4. Comparison of solution of the Prandtl model (solid line) with observations (asterisks) collected over west Greenland, 85 km inland from Kangerlussuaq (Heinemann 1999). By requiring the maximum dimensionless wind speed to be 1 and for this maximum to occur at a dimensionless height 1 we obtain the scales $U = 21.5$ m s^{-1} and $H = 120$ m.

The values of ε_V and κ_V are not well constrained beyond their order of magnitude 10^{-3}–10^{-4}. We choose them in order to constrain the Prandtl solution to pass through the maximum dimensionless velocity $u = 1$ at dimensionless height $\xi = 1$, corresponding to the Greenland data of Fig. 4. This requires us to choose

$$\varepsilon_V \approx 1.7 \times 10^{-4}, \quad \kappa_V \approx 0.9 \times 10^{-3}, \tag{2.29}$$

giving $\mathrm{Pr}_T \approx 0.2$, and

$$f^2 \approx 1.9, \quad F^2 \approx 5.5 \times 10^{-3}, \quad \nu \approx 15.3, \quad \beta \approx 1.6. \tag{2.30}$$

Allocating the upper sign to the case $h_x > 0$ and the lower sign to $h_x < 0$, the classical Prandtl solution (i.e., the limit as $f^2 \to 0$) is

$$\sqrt{\left(\frac{\beta}{\nu}\right)} u + i\tilde{T} = -i \exp\left[-\frac{(1 \pm i)}{\sqrt{2}} (\beta\nu)^{1/4} |h_x|^{1/2} \xi \right]. \tag{2.31}$$

The constraint that the maximum of u be equal to one at $\xi = 1$ requires

$$\frac{\beta}{\nu} = \frac{1}{2} e^{-\pi/2}, \quad \beta\nu = \frac{\pi^4}{64 h_x^2}, \tag{2.32}$$

and thus

$$\beta = \frac{\pi^2 e^{-\pi/4}}{8\sqrt{2}|h_x|}, \quad \nu = \frac{\pi^2 e^{\pi/4}}{4\sqrt{2}|h_x|}. \tag{2.33}$$

It is from these values (using $|h_x| = 0.25$ computed from the Greenland location in Fig. 3) that the values of β and ν are inferred, and hence the values of ε_V and κ_V are chosen.

The dimensionless wind flux is

$$\int_0^\infty u\, d\xi = -\left(\frac{\nu}{\beta^3}\right)^{1/4} \frac{\mathrm{sgn} h_x}{\sqrt{2}|h_x|^{1/2}}, \tag{2.34}$$

and we note that as $h_x \to 0$, the wind flux tends to infinity. The problem is that, if $f = 0$, in the expected physical limit where the wind speed drops to zero at a summit, the temperature Eq. (2.25) reduces to one of pure conduction, and it is impossible to satisfy the imposition of a surface temperature deficit in an infinite domain. (Note also that the solution is not too sensitive to the choice of ΔT, since it depends on ΔT through $\nu^{1/4}$, where $\nu \propto \Delta T$.)

3. The improved Prandtl model

The physical resolution of this difficulty lies in the fact that at the summit, there must be an influx of air from above to conserve that which begins to accelerate downslope. More generally, the horizontal change of wind speed with varying surface slope causes a vertical air flux.

We therefore allow u to vary with distance downslope, such that $u = u(x, \xi)$. At the top of the katabatic wind layer, the induced downward vertical velocity v_∞ is

$$v_\infty = \frac{\partial}{\partial x} \int_0^\infty u\, d\xi. \tag{3.1}$$

We retain the vertical acceleration terms in Eqs. (2.25) and (2.26) to obtain the modified system

$$\beta u h_x - \mathrm{Pr}_T f^2 v_\infty \tilde{T}_\xi = \tilde{T}_{\xi\xi}, \tag{3.2}$$

$$-f^2 v_\infty u_\xi - \nu \tilde{T} h_x = u_{\xi\xi}. \tag{3.3}$$

Note that v_∞ is unknown and is to be determined [from (3.1)]; (3.2) and (3.3) thus constitute a nonlinear system of equations.

This modification is analogous to that of the Oseen solution for slow flow past a cylinder (Ockendon and Ockendon 1995). In that case, the inertial term in the Navier–Stokes equation is always small, but crucially it is of the same size as the dominant term far from the cylinder. In the same way, the vertical advection term is always small, but becomes comparable to the conduction term near a summit. By reducing Eqs. (3.2) and (3.3) to a system of four first-order differential equations of the form

$$\boldsymbol{\nu}_\xi = \mathbf{A}\boldsymbol{\nu}, \tag{3.4}$$

where $\boldsymbol{\nu} = (u, T, u_\xi, T_\xi)^{\mathrm{T}}$, we find that there are exponential solutions

$$\boldsymbol{\nu} = c_1 \mathbf{w} \exp(\lambda_1 \xi) + \overline{c_1 \mathbf{w}} \exp(\overline{\lambda_1}\xi) + c_2 \mathbf{x} \exp(\lambda_2 \xi) + \overline{c_2 \mathbf{x}} \exp(\overline{\lambda_2}\xi), \tag{3.5}$$

where the overbars denote the complex conjugate. The exponents are solutions of the quartic equation

$$\lambda^2(\lambda + f^2 v_\infty)(\lambda + \mathrm{Pr}_T f^2 v_\infty) + \beta \nu h_x^2 = 0, \tag{3.6}$$

and occur in complex conjugate pairs; $\mathbf{w}$ and $\mathbf{x}$ are the corresponding eigenvectors.

We note from Eq. (3.6) that a simplification of the analytic solution may be found if we take $\mathrm{Pr}_T = 1$; our earlier choice of parameters gives that $\mathrm{Pr}_T \approx 0.2$, but a more physically realistic assumption is that $\mathrm{Pr}_T \gtrsim 1$ (Hinze 1959). The previous lower value may be an artificial consequence of our attempt to fit the wind profile to data (Fig. 4). In the case where $\mathrm{Pr}_T = 1$, the solutions of Eq. (3.6) are

$$\lambda = \frac{1}{2}\{-f^2 v_\infty \pm [f^4 v_\infty^2 \pm 4i(\beta\nu)^{1/2}|h_x|]^{1/2}\}. \tag{3.7}$$

We now set $P \pm iQ = [f^4 v_\infty^2 \pm 4i(\beta\nu)^{1/2}|h_x|]^{1/2}$, and suppose, without loss of generality, that $P > 0$. From the definition of P and Q we have

$$P^2 - \frac{4\beta\nu|h_x|^2}{P^2} = f^4 v_\infty^2, \quad Q = \frac{2(\beta\nu)^{1/2}|h_x|^{1/2}}{P}. \tag{3.8}$$

Note that $P > f^2 v_\infty$ and thus [since $\mathrm{Re}\,\lambda = -\frac{1}{2}(f^2 v_\infty \pm P)$ and we need $\mathrm{Re}\,\lambda < 0$ to satisfy the boundary conditions as $\xi \to \infty$] we must choose one solution to be

$$\lambda_1 = \frac{1}{2}[-f^2 v_\infty - (P + iQ)], \tag{3.9}$$

and the other exponent is simply the complex conjugate of λ_1, denoted by $\overline{\lambda_1}$. Upon calculation of the eigenvectors and application of the boundary conditions we obtain the solutions

$$u = \sqrt{\frac{\nu}{\beta}} \exp\left[-\frac{1}{2}(f^2 v_\infty + P)\xi\right] \sin\left(\frac{Q\xi}{2}\right), \tag{3.10}$$

$$\tilde{T} = -\exp\left[-\frac{1}{2}(f^2 v_\infty + P)\xi\right] \cos\left(\frac{Q\xi}{2}\right). \tag{3.11}$$

From (3.8) we have that P is defined uniquely as a monotonically increasing function of $|v_\infty|$. We define new variables $R > 0$ and V such that

$$P = (\beta\nu)^{1/4}|h_x|^{1/2}R, \quad v_\infty = \frac{1}{f^2}(\beta\nu)^{1/4}|h_x|^{1/2}V. \tag{3.12}$$

Equation (3.8) becomes

$$R^2 - \frac{4}{R^2} = V^2, \tag{3.13}$$

which defines $R = R(V)$:

$$R = \sqrt{\frac{V^2 + \sqrt{V^4 + 16}}{2}}. \tag{3.14}$$

The dimensionless katabatic wind flux, q_{kw}, is given by

$$q_{\mathrm{kw}} = \int_0^\infty u\, d\xi. \tag{3.15}$$

Using (3.10) and (3.8), we calculate

$$q_{\mathrm{kw}} = \sqrt{\frac{\nu}{\beta}}\frac{Q}{P(P + f^2 v_\infty)}. \tag{3.16}$$

Equation (3.12) then gives

$$q_{\mathrm{kw}} = \left(\frac{\nu}{\beta^3}\right)^{1/4}\frac{R - V}{2|h_x|^{1/2}}, \tag{3.17}$$

which enables us finally to calculate V and thus v_∞:

$$v_\infty = \frac{\partial}{\partial x}(q_{\mathrm{kw}}) = \left(\frac{\nu}{\beta^3}\right)^{1/4}\frac{\partial}{\partial x}\left(\frac{R - V}{2|h_x|^{1/2}}\right)$$

$$= \frac{1}{f^2}(\beta\nu)^{1/4}|h_x|^{1/2}\, V. \tag{3.18}$$

In this equation, the first equality is just (3.1), the second follows directly from (3.17), and the third uses the definition of v_∞ in (3.12). The last two terms form an ordinary differential equation for V [since $R = R(V)$]. This is to be solved subject to the condition of zero wind flux at a summit (which we take to be at $x = 0$) thus

$$q_{\mathrm{kw}} \to 0 \quad \text{as} \quad x \to 0. \tag{3.19}$$

Near summit behavior

To see whether a solution of (3.18) with (3.19) is actually possible, we consider the limiting behavior of V as $x \to 0$. As $h_x \to 0$, (3.17) implies that $R - V \to 0$. From Eq. (3.13) we can write

$$R - V = \frac{4}{R^2(R + V)}. \tag{3.20}$$

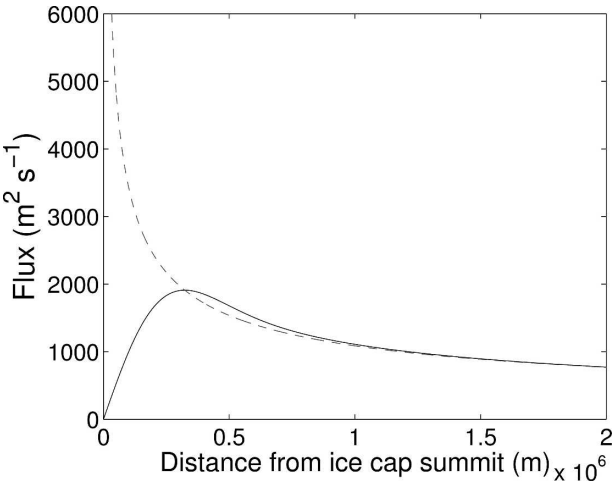

FIG. 5. Numerical result for a parabolic ice cap such that $|h_x| \propto x$. The solid line is the solution of the improved Prandtl model (3.18); the dashed line represents the classical solution (2.34). All parameter values used are those calculated for the Greenland ice cap profile, except that $n = 2$ and $m = 1$.

Since $R > V$, this requires $V \to \infty$ as $x \to 0$, and since also $R \approx V$, Eq. (3.20) gives

$$R - V \approx \frac{2}{V^3}. \tag{3.21}$$

Substituting Eq. (3.21) into Eq. (3.18) gives a first-order partial differential equation for V:

$$|h_x|^{1/2}V \approx \frac{f^2}{\beta}\frac{\partial}{\partial x}\left(\frac{1}{V^3|h_x|^{1/2}}\right). \tag{3.22}$$

This has solutions of the form $V \approx Cx^{-a}$, where C and a are constant. If we assume that the summit has a local profile given by $h(x) \approx a[1 - (1/m)x^n]$, then $|h_x| = (an/m)x^{n-1}$. Setting $\gamma = (an/m)$, we find

$$V \approx \left[\frac{f^2(n + 2)}{4\beta\gamma}\right]^{1/4} x^{-n/4}, \tag{3.23}$$

for small x, and thus

$$q_{\mathrm{kw}} \sim \left[\frac{64\nu\gamma}{(n + 2)^3 f^6}\right]^{1/4} x^{(n/4 + 1/2)}, \tag{3.24}$$

as $x \to 0$. This confirms that the local behavior of the solutions of (3.18) can be consistent with the required boundary condition (3.19).

4. Numerical results

The asymptotic form (3.24) provides a useful local approximation to start a numerical solution of (3.18). We have solved the equation using a fourth-order

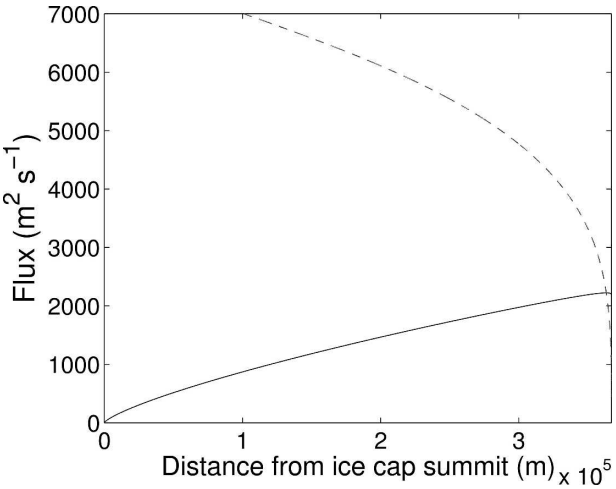

FIG. 6. Numerical result for ice cap given dimensionally by $h(x) = a[1 - (x/l)^n]^{1/m}$, where the values of a, m, and n are as previously. The origin is at the summit. The dashed line represents the solution of Prandtl's model (2.34); the solid line that of the improved model (3.18) presented here.

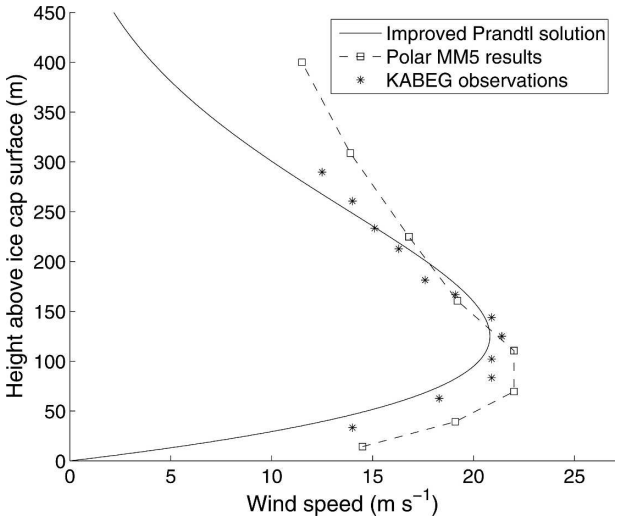

FIG. 7. Comparison of wind speed profiles, with Polar MM5 data from Fig. 12 of Bromwich et al. (2001; 0900 UTC run), and KABEG data from Fig. 10 of Heinemann (1999).

Runge–Kutta routine, but with the initial value taken from (3.24) at a small positive value of x. Before we consider the wind flux over the ice cap profile shown in Fig. 3, it is illustrative to consider a parabolic ice cap, such that $|h_x| \propto x$. Note that for such an ice cap, $n = 2$ and (3.24) implies that $q_{\mathrm{kw}} \sim x$, as can be seen in Fig. 5. This figure shows that, close to the summit, the agreement between the basic and improved Prandtl models is poor. At a distance of approximately 400 km from the summit, the agreement becomes good; while at 1000 km (a suitable scale width for Antarctica, e.g.), the solution to the improved model has relaxed to the Prandtl solution and the agreement is excellent.

For the wind flux over the Greenland cross section (Fig. 6) we see that the solutions to the classical and improved models do not agree at any point. Close to the summit, the wind flux given by the classical model is infinite; it then decreases as the ice cap is descended before becoming zero at the ice cap edge. In contrast, the wind flux given by the improved model starts close to zero and then increases almost linearly as the ice cap is descended. At the ice cap edge, there is a finite, nonzero wind flux. The relaxation seen in Fig. 5 is not seen for this profile because of the shorter length scale and the infinite gradient at the ice cap edge.

As the parameter values have been chosen to provide the best fit of the Prandtl model to the data at the location of the data collected, it is unsurprising that the improved model does not fit the data exactly, although it can be seen to have the correct shape. We therefore modify our choice of U and H such that $U = 24\ \mathrm{m\ s^{-1}}$ and $H = 240$ m (which enables the numerical output to fit the Greenland data), while fixing the values of $\beta = 1.6$, $f^2 = 1.9$, $\mathrm{Pr}_T = 1$, and $\nu = 15.3$. This therefore modifies the values of the remaining parameters such that

$$\varepsilon_V \approx 3.4 \times 10^{-4}, \quad \kappa_V \approx 3.4 \times 10^{-4},$$
$$\delta \approx 5.4 \times 10^{-2}, \quad N \approx 7.2 \times 10^{-3}\ \mathrm{s^{-1}}, \qquad (4.1)$$

which are comparable to the values used previously.

We now compare the improved solution [with the new parameter values given in (4.1)] with observations collected over Greenland during the KABEG'97 experiment, and numerical output from the Polar MM5 model. The KABEG'97 data on the vertical wind and potential temperature structures was collected by aircraft ascents and descents over the ice sheet. A description of the MM5 model may be found in Grell et al. (1994), and its modification for use in polar regions is described in Bromwich et al. (2001).

Here we use data collected during the flight on 13 May 1997 at the point marked in Fig. 3 [see Heinemann (1999), Fig. 10, flight Tpu]. For this flight there was a strong synoptic forcing caused by a high pressure system over the interior of the ice sheet; this acted to support katabatic wind development. This was also one of the flights for which conditions were best simulated by the Polar MM5 model (Bromwich et al. 2001, Fig. 12).

Figure 7 shows a comparison of observed, computed (with Polar MM5) and the improved Prandtl wind speed profiles. The improved Prandtl model fits the data reasonably well, despite its oversimplistic assump-

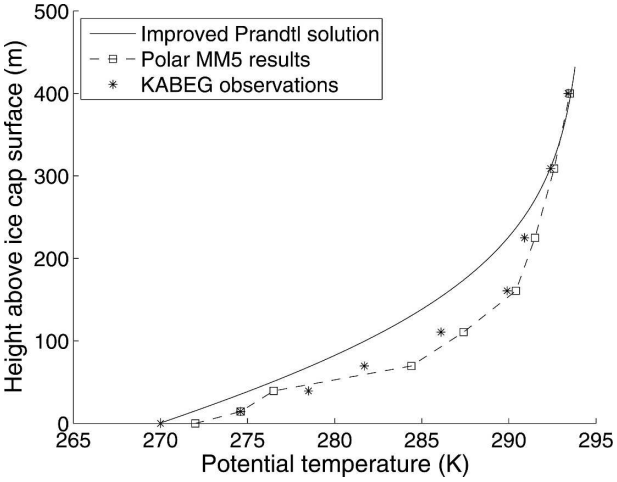

FIG. 8. Comparison of potential temperature profiles, with polar MM5 data from Fig. 12 of Bromwich et al. (2001; 0900 UTC run), Bromwich et al. (2001), and KABEG data from Fig. 10 of Heinemann (1999). To fit this particular dataset, we chose $T_0 = 288.5$ K and $\Delta T = 18.5$ K, giving a value of $\delta = 6.4 \times 10^{-4}$.

tions, but the gradient of the wind speed is overestimated above the katabatic jet.

The results for potential temperature are shown in Fig. 8. It is clear that the numerical output here is a far better match to observations than the solution to the improved Prandtl model, which, although having the correct value at the surface and the correct potential temperature gradient near the top of the katabatic wind layer, underestimates the potential temperature. The match could perhaps be improved by incorporating a vertically varying eddy diffusivity.

5. Conclusions

In this paper, we have derived the classical Prandtl model for slope wind flow. We have detailed the problems the model has in reproducing sharp near-surface gradients because of its assumption of constant mixing length, and shown that, as the slope tends to zero, the wind flux becomes infinite. We then derived an improved model, in the spirit of the Oseen approximation, in which vertical acceleration terms are retained. In this case, there is still an analytic solution and we have compared this with both observations and numerical model output.

Upon performing such a comparison, we find that the improved model matches the data well. We also find that the improved model simulates the near surface gradients well, although still having a gradient that is too steep below the katabatic wind maximum, without the need for a vertically varying eddy diffusivity. An extension to this work would be incorporation of such an eddy diffusivity into the improved Prandtl model, in line with the work of Grisogono and Oerlemans (2001).

Another useful extension would be to consider the effects of Coriolis terms. This has been done for the Prandtl model by Stiperski et al. (2007), and is important since numerical models show a spiralling of the katabatic wind streamlines to the left over Antarctica (Parish and Bromwich 1987). As discussed earlier, Coriolis terms are likely to be of importance over length scales in excess of 300 km.

In summary, we have found that by retaining the vertical acceleration terms in Prandtl's (1952) model for slope winds it is possible to obtain a solution that allows for variations in slope. The physical justification for this is that, at a summit where the slope is zero, there must be an influx of air from above in order for mass to be conserved. The vertical acceleration terms are always small, but near a summit they are of the same size as the conduction terms, and it is therefore no longer appropriate to neglect them. The improved model exhibits a similar behavior to the classical model, but is slightly better at reproducing the near-surface gradients observed.

Acknowledgments. R. J. Z. acknowledges the support of an EPSRC studentship; A. C. F. acknowledges the continuing support of the University of Limerick.

REFERENCES

Ball, F. K., 1956: The theory of strong katabatic winds. *Aust. J. Phys.,* **9,** 373–386.

——, 1960: Winds on the ice slopes of Antarctica. *Antarctic Meteorology, Proceedings of the Symposium on Antarctic Meteorology, Melbourne, 1959,* Pergamon Press, 9–16.

Bamber, J. L., R. L. Layberry, and S. P. Gogenini, 2001: A new ice thickness and bed data set for the Greenland ice sheet 1: Measurement, data reduction, and errors. *J. Geophys. Res.,* **106** (D24), 33 773–33 780.

Bender, C. M., and S. A. Orszag, 1978: *Advanced Mathematical Methods for Scientists and Engineers.* McGraw-Hill, 593 pp.

Bromwich, D. H., D. Yang, and K. M. Hines, 1996: Wintertime surface winds over the Greenland Ice Sheet. *Mon. Wea. Rev.,* **124,** 1941–1947.

——, J. J. Cassano, T. Klein, G. Heinemann, K. M. Hines, K. Steffen, and J. E. Box, 2001: Mesoscale modeling of katabatic winds over Greenland with the polar MM5. *Mon. Wea. Rev.,* **129,** 2290–2309.

Davolio, S., and A. Buzzi, 2002: Mechanisms of Antarctic katabatic currents near Terra Nova Bay. *Tellus,* **54A,** 187–204.

Fowler, A. C., 2005: Mathematics and the environment. Lecture Notes, Mathematical Institute, University of Oxford, 234 pp.

Grell, G. A., J. Dudhia, and D. R. Stauffer, 1994: A description of the fifth-generation Penn State/NCAR Mesoscale Model (MM5). NCAR Tech. Note NCAR/TN-398+STR, 122 pp.

Grisogono, B., 2003: Post-onset behaviour of the pure katabatic flow. *Bound.-Layer Meteor.,* **107,** 157–175.

——, and J. Oerlemans, 2001: Katabatic flow: Analytic solutions for gradually varying eddy diffusivities. *J. Atmos. Sci.,* **58,** 3349–3356.

——, and ——, 2002: Justifying the WKB approximation in pure katabatic flows. *Tellus,* **54A,** 453–462.

Heinemann, G., 1999: The KABEG '97 field experiment: An aircraft-based study of katabatic wind dynamics over the Greenland ice sheet. *Bound.-Layer Meteor.,* **93,** 75–116.

——, and T. Klein, 2002: Modelling and observations of the katabatic flow dynamics over Greenland. *Tellus,* **54A,** 542–554.

Hinze, J. O., 1959: *Turbulence: An Introduction to Its Mechanism and Theory.* McGraw-Hill, 586 pp.

Hootman, B. W., and W. Blumen, 1983: Analysis of nighttime drainage winds in Boulder, Colorado, during 1980. *Mon. Wea. Rev.,* **111,** 1052–1061.

King, J. C., 1989: Low-level wind profiles at an Antarctic coastal station. *Antarct. Sci.,* **1,** 169–178.

——, and J. Turner, 1997: *Antarctic Meteorology and Climatology.* Cambridge University Press, 409 pp.

Layberry, R. L., and J. L. Bamber, 2001: A new ice thickness and bed data set for the Greenland ice sheet 2. Relationship between dynamics and basal topography. *J. Geophys. Res.,* **106** (D24), 33 781–33 788.

Lefebre, F., X. Fettweis, H. Gallée, J.-P. van Ypersele, P. Marbaix, W. Greuell, and P. Calanca, 2005: Evaluation of a high-resolution regional climate simulation over Greenland. *Climate Dyn.,* **25,** 99–116.

Nappo, C. J., and K. S. Rao, 1987: A model study of pure katabatic flows. *Tellus,* **39A,** 61–71.

Ockendon, H., and J. R. Ockendon, 1995: *Viscous Flow.* Cambridge University Press, 113 pp.

Oerlemans, J., and B. Grisogono, 2002: Glacier winds and parameterisation of the related surface heat fluxes. *Tellus,* **54A,** 440–452.

Parish, T. R., and D. H. Bromwich, 1987: The surface windfield over the Antarctic ice sheets. *Nature,* **328,** 51–54.

——, and K. T. Waight III, 1987: The forcing of Antarctic katabatic winds. *Mon. Wea. Rev.,* **115,** 2214–2226.

——, and J. J. Cassano, 2003: Diagnosis of the katabatic wind influence on the wintertime Antarctic surface wind field from numerical simulations. *Mon. Wea. Rev.,* **131,** 1128–1139.

Parmhed, O., J. Oerlemans, and B. Grisogono, 2004: Describing surface fluxes in katabatic flow over Breidamerkurjökull, Iceland. *Quart. J. Roy. Meteor. Soc.,* **130,** 1137–1151.

Paterson, W. B., 1994: *The Physics of Glaciers.* Pergamon, 480 pp.

Pedlosky, J., 1979: *Geophysical Fluid Dynamics.* Springer-Verlag, 626 pp.

Prandtl, L., 1952: *Essentials of Fluid Dynamics: With Applications to Hydraulics, Aeronautics, Meteorology and Other Subjects* (English translation). Blackie and Son, 452 pp.

Rao, K. S., and H. F. Snodgrass, 1981: A nonstationary nocturnal drainage model. *Bound.-Layer Meteor.,* **20,** 309–320.

Renfrew, I. A., 2004: The dynamics of idealized katabatic flow over a moderate slope and ice shelf. *Quart. J. Roy. Meteor. Soc.,* **130,** 1023–1045.

——, and P. S. Anderson, 2002: The surface climatology of an ordinary katabatic wind regime in Coats Land, Antarctica. *Tellus,* **54A,** 463–484.

Skyllingstad, E. D., 2003: Large-eddy simulation of katabatic flows. *Bound.-Layer Meteor.,* **106,** 217–243.

Stiperski, I., I. Kavčič, B. Grisogono, and D. R. Durran, 2007: Including Coriolis effects in the Prandtl model for katabatic flow. *Quart. J. Roy. Meteor. Soc.,* **133,** 101–106.

Van Lipzig, N. P. M., J. Turner, S. R. Colwell, and M. R. van den Broeke, 2004: The near-surface wind field over the Antarctic continent. *J. Climatol.,* **24,** 1973–1982.